Centralized Collaborative Sparse Unmixing for Hyperspectral Images

Rui Wang, Heng-Chao Li, *Senior Member, IEEE*, Wenzhi Liao, *Senior Member, IEEE*, Xin Huang, *Senior Member, IEEE*, and Wilfried Philips, *Senior Member, IEEE*

***Abstract*—Spectral unmixing is very important in hyperspectral image analysis and processing, which aims at identifying the constituent spectra (i.e., endmembers) and estimating their fractional abundances from the mixed pixels. In recent years, sparse unmixing has received considerable interest. However, the acquired hyperspectral images are generally degraded by the noise, making sparse unmixing not faithful enough. To address this issue, this paper proposes a novel framework to couple sparse hyperspectral unmixing and abundance estimation error reduction together. Specifically, with the definition of abundance estimation error, a centralized constraint is incorporated into the collaborative sparse unmixing framework by exploiting the nonlocal redundancy of abundance map. This way we suppress the abundance estimation error, and improve the unmixing accuracy. Meanwhile, the alternating direction method of multipliers is introduced to solve the underlying constrained model. Experimental results on both synthetic and real hyperspectral data demonstrate the effectiveness of our proposed algorithm.**

***Index Terms*—Abundance estimation error, hyperspectral images, nonlocal means (NLM), spectral unmixing.**

I. Introduction

HYPERSPECTRAL imaging collects and processes information from across the electromagnetic spectrum. The resulting hyperspectral images contain a wealth of high-resolution spectral information permitting various applications in the field of geoinformation science and earth observation. However, because of the limited spatial resolution, together with microscopic material mixing and multiple scattering, the mixed pixels widely appear in the observed hyperspectral data. Therefore, spectral unmixing is an important technique for hyperspectral image exploitation, which tends to identify the constituent spectra (i.e., endmembers) and estimate their fractional abundances from the mixed pixel [1].

In the context of spectral unmixing, both linear and nonlinear mixture models are utilized to describe the mixing process of mixed pixels [2], [3], among which the former has attracted significant interest of researchers in terms of its simplicity and definite physical meaning. Specifically, the linear mixture model (LMM) [2] assumes that the measured spectral signature can be modeled as a linear combination of the endmembers weighted by their fractional abundances. To date, many unmixing approaches based on LMM have been proposed from the geometrical or statistical perspective [2]. The geometrical class of approaches conjectures that the spectral vectors lie in a simplex whose vertices correspond to the endmembers. The classical unmixing algorithms assume the presence of pure pixels in the hyperspectral data, which start with endmember extraction, and then perform abundance estimation by decomposing the mixed pixels with the nonconstrained or constrained least-squares methods [4]. To identify the endmembers, N-FINDR [5] and vertex component analysis (VCA) [6] are commonly used. Specifically, N-FINDR finds the endmembers by searching for a simplex with the maximum volume, whereas VCA iteratively extracts them by the projection analysis. Nevertheless, they usually do not perform well in practice due to that the pure pixel assumption can barely be fulfilled at most time. Therefore, the minimum volume-based geometric approaches, such as minimum volume simplex analysis (MVSA) [7] and minimum volume enclosing simplex (MVES) [8], have been proposed to deal with the scenarios of no pure pixels. The basic idea is to fit a simplex of minimum volume to the hyperspectral data for endmember extraction [9], which amounts to solving the constrained optimization problem. The difference between MVSA and MVES lies in the optimization strategy. Besides the high computational complexity, these algorithms are likely to fail in highly mixed data because there are not enough spectral vectors in the simplex facets.

The statistical class of approaches that exploits Bayesian paradigm to provide a natural framework for representing variability in endmembers tends to simultaneously obtain the endmembers and their corresponding abundances. In [10], a fully Bayesian algorithm was proposed to generate the unmixing results by imposing prior distributions on the model variables to account for the nonnegativity and full additivity constraints. In addition, the unmixing algorithms of blind source separation, e.g., independent component analysis (ICA) [11] and

Manuscript received April 8, 2016; revised August 7, 2016, October 24, 2016, and December 25, 2016; accepted January 1, 2017. Date of publication February 5, 2017; date of current version April 10, 2017. This work was supported in part by the National Natural Science Foundation of China under Grant 61371165, and in part by FWO (Fund for Scientific Research in Flanders, Belgium) project G037115N: Data Fusion for Image Analysis in Remote Sensing. *(Corresponding author: Heng-Chao Li.)*

R. Wang and H.-C. Li are with the Sichuan Provincial Key Laboratory of Information Coding and Transmission, Southwest Jiaotong University, Chengdu 610031, China (e-mail: wangruinew@163.com; lihengchao_78@163.com).

W. Liao and W. Philips are with the Department of Telecommunications and Information Processing, Ghent University, Ghent 9000, Belgium (e-mail: wliao@telin.ugent.be; philips@telin.ugent.be).

X. Huang is with the School of Remote Sensing and Information Engineering, Wuhan University, Wuhan 430079, China (e-mail: huang_whu@163.com).

Color versions of one or more of the figures in this paper are available online at http://ieeexplore.ieee.org.

Digital Object Identifier 10.1109/JSTARS.2017.2651063

1939-1404 © 2017 IEEE. Personal use is permitted, but republication/redistribution requires IEEE permission.
See http://www.ieee.org/publications_standards/publications/rights/index.html for more information.

nonnegative matrix factorization (NMF) [12], are also considered to belong to the statistical approaches [2]. ICA supposes the spectral components to be statistically independent. But this assumption goes against the abundance sum-to-one constraint (ASC) in LMM, which degrades the performance of ICA in unmixing. Different from ICA, NMF decomposes the hyperspectral data into two nonnegative matrices (respectively corresponding to the endmember matrix and the abundance matrix), being subjected to the nonnegative constraint. This nonnegative constraint naturally ensures the abundance nonnegativity constraint (ANC) in LMM, thus making NMF applicable for hyperspectral unmixing. But due to the nonconvexity of the objective function, NMF may find some local minimum solutions as the final results [12]. To address this issue, many extended NMF algorithms have been proposed in the literature [13]–[16], whose unmixing performance, however, is still susceptible to the initial setting and the noise disturbance.

Besides that some require the presence of pure materials, all the aforementioned algorithms need to estimate the number of endmembers in advance for a given scene before performing the unmixing procedure. To sidestep these two obstacles, sparse unmixing is successfully proposed as a new paradigm to characterize the mixed pixels by finding the optimal subset of signatures from a (potentially very large) spectral library in a semisupervised fashion [17], [18]. It opens up new perspectives to perform spectral unmixing. The sparse unmixing algorithm via variable splitting and augmented Lagrangian (SUnSAL) [18] and the collaborative SUnSAL (CLSUnSAL) [19] are two of the most popular sparse unmixing methods. Recently, more efforts have been devoted to incorporating the spatial-contextual information into sparse unmixing algorithms to obtain much better results [20], [21]. In [20], SUnSAL-TV includes a total variation (TV) regularizer to promote spatial homogeneity among neighboring pixels. However, SUnSAL-TV may lead to oversmoothness and blurred boundaries. Nonlocal sparse unmixing (NLSU) [21] takes into account the nonlocal spatial information of the whole abundance image, and enables better unmixing performances than SUnSAL-TV. Both approaches model the spatial information on the estimated abundances. However, due to the noise (which cannot be avoided during the acquisition of the hyperspectral data), the estimated abundances are often inaccurate and variable, leading to unfaithful spatial information modeling. In order to overcome the noise effect, an improved NLSU algorithm is recently proposed in [22]. It first applies the noise-adjusted principal component analysis (NAPCA) [23] for noise reduction and information extraction, and then characterizes the spatial relationships based on the first principal component instead of the estimated abundances. However, the spatial relationships obtained from one extracted component are not reliable.

In this paper, we propose a centralized collaborative sparse unmixing (CCSU) algorithm to address the aforementioned issues, for which sparse unmixing and abundance estimation error reduction are coupled together in a unified framework. Specifically, abundance estimation error is first defined by calculating the difference between the estimated abundance of noisy data and the desired abundance of original data. To make it measurable, the nonlocal spatial information is exploited to yield a good approximation of desired abundance, which is implemented in an iterative manner such that the reconstructed hyperspectral data after each iteration contains less noise than those in the previous iterations, and can benefit the patch searching and the approximation quality. Since the abundance estimation error is generated during the process of sparse unmixing, it will affect the efficiency of hyperspectral sparse unmixing. We then take the abundance estimation error into account in our sparse unmixing model by a centralized constraint. The abundance is finally optimized by the alternating direction method of multipliers (ADMM).

The remainder of this paper is organized as follows. In Section II, we introduce the related work of sparse unmixing. Section III is devoted to the development of the proposed unmixing algorithm. Experimental results are reported in Section IV, followed by concluding remarks in Section V.

II. Related Work

Let $\mathbf{A} \in \mathbb{R}^{L\times m}$ denote a spectral library having m spectral signatures of L bands. Instead of the spectral endmembers directly extracted or generated from the hyperspectral data, linear sparse unmixing amounts to finding the optimal subset of spectral samples in $\mathbf{A}$ to best model each mixed pixel in the scene. Typically, we have

$$\mathbf{y} = \mathbf{A}\mathbf{x} + \mathbf{n} \tag{1}$$

where $\mathbf{y} \in \mathbb{R}^{L\times 1}$ is the observed spectral vector, $\mathbf{x} \in \mathbb{R}^{m\times 1}$ denotes the fractional abundance vector with regard to the library $\mathbf{A}$, still being subject to two physical constraints: ANC and ASC (i.e., $\mathbf{x} \geq 0$ and $\sum_{p=1}^{m} x_p = 1$). Here, only a few of the signatures contained in $\mathbf{A}$ are likely contributing to the observed mixed pixel such that $\mathbf{x}$ contains many values of zeros (i.e., it is *sparse*).

In conventional sparse unmixing methods, the optimization problems can be formulated as following:

$$\min_{\mathbf{X}} \frac{1}{2}\|\mathbf{Y} - \mathbf{A}\mathbf{X}\|_F^2 + \lambda\|\mathbf{X}\|_{\rho,1} + \gamma TV(\mathbf{X}), \quad \text{s.t. } \mathbf{X} \geq 0 \tag{2}$$

where $\mathbf{Y} = [\mathbf{y}_1, \ldots, \mathbf{y}_n] \in \mathbb{R}^{L\times n}$, and $\mathbf{X} = [\mathbf{x}_1, \ldots, \mathbf{x}_n] \in \mathbb{R}^{m\times n}$ are observed data and the abundance matrix, n is the number of the pixels in the image. Specifically, $\| \bullet \|_F$ is the Frobenius norm.

1) By setting $\gamma = 0$ and $\rho = 1$, we refer to (2) as SUnSAL [17]. In SUnSAL, $\|\mathbf{X}\|_{1,1} = \sum_{j=1}^{n} \|\mathbf{x}_j\|_1$ as $\mathbf{x}_j$ denotes the jth column of $\mathbf{X}$.
2) Similarly, $\gamma = 0$ and $\rho = 2$ result in CLSUnSAL [19]. In CLSUnSAL, $\|\mathbf{X}\|_{2,1} = \sum_{p=1}^{m} \|\mathbf{x}^p\|_2$ with $\mathbf{x}^p$ being the pth row of $\mathbf{X}$ denotes the $l_{2,1}$ mixed norm that promotes sparsity among the lines of $\mathbf{X}$.
3) We term the problem of (2) with $\gamma \neq 0$ and $\rho = 1$ as SUnSAL-TV [20], in which, $\mathrm{TV}(\mathbf{X}) \equiv \sum_{i,j\in\varepsilon} \|\mathbf{x}_i - \mathbf{x}_j\|$ is a vector extension of the nonisotropic TV, with the functionality of increasing piecewise smoothness on $\mathbf{X}$.

III. CCSU Algorithm

This section details our proposed CCSU algorithm. We start with the definition of an abundance estimation error, and then construct our unmixing model by considering abundance estimation error, followed by the abundance optimization via ADMM.

A. Proposed CCSU Model

In the scenario of spectral unmixing, the acquired hyperspectral image represents a degraded version of the original spectral reflectance contaminated by additive noise, modeled as

$$\mathbf{Y} = \mathbf{Z} + \mathbf{N} \tag{3}$$

where $\mathbf{Y} \in \mathbb{R}^{L\times n}$, $\mathbf{Z} \in \mathbb{R}^{L\times n}$, and $\mathbf{N} \in \mathbb{R}^{L\times n}$ are observed data matrix, original data matrix, and noise matrix, respectively. Ideally, the desired abundance matrix is denoted as $\mathbf{X}^*$, which is estimated from the original hyperspectral data $\mathbf{Z}$ by optimizing

$$\min_{\mathbf{X}^*} \frac{1}{2}\|\mathbf{Z} - \mathbf{A}\mathbf{X}^*\|_F^2 + \lambda\|\mathbf{X}^*\|_{2,1}, \quad \text{s.t. } \mathbf{X}^* \geq 0. \tag{4}$$

Since $\mathbf{Z}$ is not available, the unmixing will be implemented on $\mathbf{Y}$ to obtain the abundance matrix $\mathbf{X}$ from the formulation of (4) by substituting $\mathbf{Y}$ for $\mathbf{Z}$. For an effective sparse unmixing, $\mathbf{X}$ is expected to be as close as possible to $\mathbf{X}^*$. However, due to the noise degradation as well as the high mutual coherence of library $\mathbf{A}$, $\mathbf{X}$ may deviate much from $\mathbf{X}^*$, yielding an inaccurate unmixing result. Here, we define the abundance estimation error as the difference between $\mathbf{X}$ and $\mathbf{X}^*$

$$\mathbf{V} = \mathbf{X} - \mathbf{X}^*. \tag{5}$$

Obviously, abundance estimation error cannot be avoided during the process of sparse unmixing, and will affect the efficiency of spectral unmixing. With the definition of (5), the estimation quality of $\mathbf{X}$ can be improved by suppressing $\mathbf{V}$. Therefore, the objective of this paper is to minimize the $\mathbf{V}$, making the estimated abundance $\mathbf{X}$ (from the observed hyperspectral data) as closer as the desired abundance $\mathbf{X}^*$.

However, in many applications, it is scarce to obtain the original hyperspectral data, which indicate $\mathbf{X}^*$ is almost unavailable, leading to unmeasured $\mathbf{V}$ directly. Nonetheless, if we have some reasonable estimation of $\mathbf{X}^*$, denoted by $\widehat{\mathbf{X}}$, we can utilize $\mathbf{X} - \widehat{\mathbf{X}}$ to approximate $\mathbf{V}$, thus making it measurable. Obviously, the accuracy of $\widehat{\mathbf{X}}$ determines the approximation quality. As we know, there are many nonlocal repetitive materials across an observed scene, which have similar spectral and spatial structures. Such nonlocal redundancy is very helpful to improve the accuracy of the estimated $\widehat{\mathbf{X}}$. With the assumption of sharing the same active set of endmembers for all the observed pixels, pixels with similar spectral characteristic in the hyperspectral image typically have the similar fractional abundances. As such, we take advantage of the nonlocal means (NLM) method to yield $\widehat{\mathbf{X}}$ by exploiting nonlocal spatial information, which was first proposed for image denoising [24] and recently has been extended for hyperspectral applications [25], [26]. Suppose $\widehat{\mathbf{X}} = [\widehat{\mathbf{x}}_1, \ldots, \widehat{\mathbf{x}}_n] \in \mathbb{R}^{m\times n}$ is an approximation of $\mathbf{X}^*$, i.e., $\widehat{\mathbf{X}} \approx \mathbf{X}^*$. For a given pixel $\mathbf{y}_j$ from the observed hyperspectral data, we search for a set of its similar pixels Ω_j (as illustrated in Fig. 1) in the whole image (or in a sufficiently large window around $\mathbf{y}_j$) according to the similarity between the three-dimensional (3-D) patch Δ_j centered at $\mathbf{y}_j$ and its nonlocal 3-D patches $\Delta_{k\in[1,K]}$ (as illustrated in Fig. 1), defined as

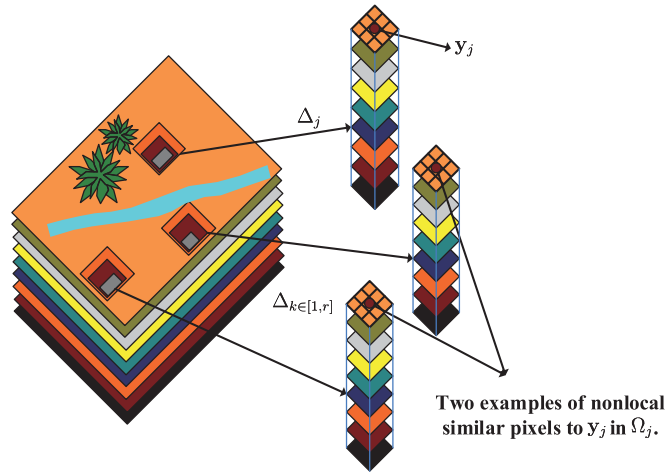

Fig. 1. Diagram of nonlocal similar pixels for any given pixel $\mathbf{y}_j$, whose search process is implemented by 3-D patch matching.

$$\|\Delta_j - \Delta_k\| = \sum_{s=1}^{L} \big(I_j(s) - I_k(s)\big) \otimes \Theta \tag{6}$$

where $I_j(s)$ and $I_k(s)$ are the vector formulations of hyperspectral image patches Δ_j and Δ_k in the sth band, $\otimes$ is the convolution operator and Θ is a Gaussian blur kernel. Specifically, we reshape the 2-D patches of Δ_j and Δ_k in the sth band to generate $I_j(s)$ and $I_k(s)$. The Gaussian blur kernel Θ is a spatial convolution kernel which measures the weights of the corresponding pixels, whose value is given by

$$\mathbf{\Theta} = \begin{bmatrix} \frac{1}{16} & \frac{1}{8} & \frac{1}{16} \\ \frac{1}{8} & \frac{1}{4} & \frac{1}{8} \\ \frac{1}{16} & \frac{1}{8} & \frac{1}{16} \end{bmatrix}. \tag{7}$$

The first K most similar patches are chosen based on the K minimum distances between Δ_j and other 3-D patches in the search window around $\mathbf{y}_j$ calculated by (6) such that we can construct Ω_j with their central pixels. Then, having $\mathbf{X} = [\mathbf{x}_1, \ldots, \mathbf{x}_n]$ given by the initialization or estimated in the previous iteration, the approximated $\widehat{\mathbf{x}}_j$ can be computed as the weighted average of the abundances associated with the similar pixels in Ω_j, i.e.,

$$\widehat{\mathbf{x}}_j = \sum_{q\in\Omega_j} \omega_{j,q}\mathbf{x}_q. \tag{8}$$

Here $\omega_{j,q}$ denotes the NLM weight, which can be calculated by

$$\omega_{j,q} = \frac{1}{C}\exp\left\{-\frac{\|\widehat{\mathbf{z}}_j - \widehat{\mathbf{z}}_q\|_2^2}{h}\right\} \tag{9}$$

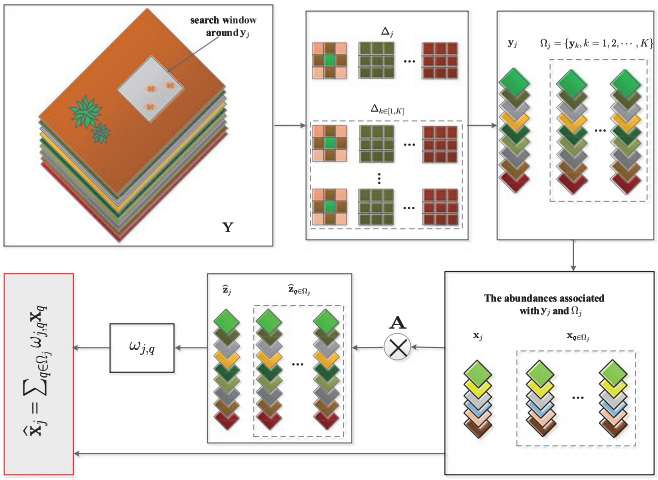

Fig. 2. Example of illustration for estimation procedure of $\widehat{\mathbf{x}}_j$.

where $C = \sum_{q\in\Omega_j} \exp\left\{-\frac{\|\widehat{\mathbf{z}}_j - \widehat{\mathbf{z}}_q\|_2^2}{h}\right\}$ is a normalization factor, h is a predetermined scalar, and $\widehat{\mathbf{z}}_j = \mathbf{A}\mathbf{x}_j$ and $\widehat{\mathbf{z}}_q = \mathbf{A}\mathbf{x}_q$ are the approximations of original spectra $\mathbf{z}_j$ and $\mathbf{z}_{q\in\Omega_j}$, respectively. An example of illustration for estimation procedure of $\widehat{\mathbf{x}}_j$ is shown in Fig. 2.

To suppress the abundance estimation error and improve the unmixing quality, we propose a CCSU model as

$$\min_{\mathbf{X}} \frac{1}{2}\|\mathbf{Y} - \mathbf{A}\mathbf{X}\|_F^2 + \lambda\|\mathbf{X}\|_{2,1} + \gamma\|\mathbf{X} - \widehat{\mathbf{X}}\|_1, \quad \text{s.t. } \mathbf{X} \geq 0 \tag{10}$$

where γ and λ are regularization parameters. The third term of (10) is the centralized constraint, which enforces the sparse unmixing abundance $\mathbf{X}$ to approach its NLM estimate. Abundance estimation error is reduced iteratively, thus improving the accuracy of the estimated abundance. Similar constraint has already been applied in image restoration [27]. Mathematically, the optimization problem of (10) can be rewritten as

$$\min_{\mathbf{X}} \frac{1}{2}\|\mathbf{Y} - \mathbf{A}\mathbf{X}\|_F^2 + \lambda\|\mathbf{X}\|_{2,1} + \gamma\|\mathbf{X} - \widehat{\mathbf{X}}\|_1 + \iota_{R_+}(\mathbf{X}) \tag{11}$$

where $\iota_{R_+}(\mathbf{X}) = \sum_{j=1}^{n} \iota_{R_+}(\mathbf{x}_j)$ is the indicator function with $\iota_{R_+}(\mathbf{x}_j) = 0$ when $\mathbf{x}_j$ belongs to the nonnegative orthant, otherwise $\iota_{R_+}(\mathbf{x}_j) = +\infty$.

With $\widehat{\mathbf{X}}$ in hand, we can optimize the estimated abundance $\mathbf{X}$ iteratively by solving the objective function of (11). After each iteration, a newly reconstructed hyperspectral data $\widehat{\mathbf{Z}}^{(t)} = \mathbf{A}\mathbf{X}^{(t)}$ can be obtained, which contains less noise than those $(\widehat{\mathbf{Z}}^{(t-1)}, \widehat{\mathbf{Z}}^{(t-2)}, \ldots)$ in the previous iterations. To improve the approximation quality, we recalculate $\widehat{\mathbf{X}}$ (i.e., $\widehat{\mathbf{X}}^{(t)}$) by better searching the nonlocal patches in $\widehat{\mathbf{Z}}^{(t)}$ with the spatial–spectral similarity of (6). As such, our proposed unmixing method ensures the estimated abundance $\mathbf{X}^{(t)}$ become closer and closer to the desired abundance $\mathbf{X}^*$ through $\mathbf{V}^{(t)}$, i.e., $\|\mathbf{V}^{(t)}\|_1 \leq \|\mathbf{V}^{(t-1)}\|_1$.

B. Optimization With the ADMM

To solve (11), we adopt the ADMM [28] in such a way that the difficult problem of (11) is decomposed into a sequence of simpler ones [17], [29], [30]. The ADMM, originally proposed in [28], has emerged recently as a flexible and efficient tool for convex optimization. Specifically, the proposed optimization problem (11) can be equivalently formulated as

$$\begin{aligned} \min_{\mathbf{X},\mathbf{V_1},\mathbf{V_2},\mathbf{V_3},\mathbf{V_4}} & \frac{1}{2}\|\mathbf{Y} - \mathbf{V_1}\|_F^2 + \lambda\|\mathbf{V_2}\|_{2,1} \\ & + \gamma\|\mathbf{V_3} - \widehat{\mathbf{X}}\|_1 + \iota_{R_+}(\mathbf{V_4}) \\ \text{s.t.} \quad & \mathbf{V}_1 = \mathbf{A}\mathbf{X}, \mathbf{V}_2 = \mathbf{X}, \mathbf{V}_3 = \mathbf{X}, \mathbf{V}_4 = \mathbf{X}. \end{aligned} \tag{12}$$

Then, (12) can be further expressed in a compact form

$$\min_{\mathbf{X},\mathbf{V}} g(\mathbf{V}) \quad \mathbf{G}\mathbf{X} + \mathbf{B}\mathbf{V} = 0 \tag{13}$$

where $\mathbf{V} = (\mathbf{V_1}, \mathbf{V_2}, \mathbf{V_3}, \mathbf{V_4})$, $g(\mathbf{V}) = \frac{1}{2}\|\mathbf{Y} - \mathbf{V_1}\|_F^2 + \lambda\|\mathbf{V_2}\|_{2,1} + \gamma\|\mathbf{V_3} - \widehat{\mathbf{X}}\|_1 + \iota_{R_+}(\mathbf{V_4})$, and $\mathbf{G}$ and $\mathbf{B}$ are, respectively, given by

$$\mathbf{G} = \begin{bmatrix} \mathbf{A} \\ \mathbf{I} \\ \mathbf{I} \\ \mathbf{I} \end{bmatrix}, \quad \mathbf{B} = \begin{bmatrix} -\mathbf{I} & 0 & 0 & 0 \\ 0 & -\mathbf{I} & 0 & 0 \\ 0 & 0 & -\mathbf{I} & 0 \\ 0 & 0 & 0 & -\mathbf{I} \end{bmatrix}. \tag{14}$$

By introducing the scaled Lagrange multipliers $\mathbf{D} = (\mathbf{D_1}, \mathbf{D_2}, \mathbf{D_3}, \mathbf{D_4})$, the augmented Lagrangian associated with the optimization of (13) is written as

$$\begin{aligned} \mathcal{L}(\mathbf{X}, \mathbf{V}, \mathbf{D}) &\equiv g(\mathbf{V}) + \frac{\mu}{2}\|\mathbf{G}\mathbf{X} + \mathbf{B}\mathbf{V} - \mathbf{D}\|_F^2 \\ &= \frac{1}{2}\|\mathbf{V}_1 - \mathbf{Y}\|_F^2 + \lambda\|\mathbf{V_2}\|_{2,1} + \gamma\|\mathbf{V_3} - \widehat{\mathbf{X}}\|_1 \\ &\quad + \iota_{R+}(\mathbf{V}_4) + \frac{\mu}{2}\|\mathbf{A}\mathbf{X} - \mathbf{V}_1 - \mathbf{D}_1\|_F^2 \\ &\quad + \frac{\mu}{2}\|\mathbf{X} - \mathbf{V}_2 - \mathbf{D}_2\|_F^2 + \frac{\mu}{2}\|\mathbf{X} - \mathbf{V}_3 - \mathbf{D}_3\|_F^2 \\ &\quad + \frac{\mu}{2}\|\mathbf{X} - \mathbf{V}_4 - \mathbf{D}_4\|_F^2. \end{aligned} \tag{15}$$

with $\mu > 0$ being a penalty parameter. The ADMM iteratively minimizes $\mathcal{L}(\mathbf{X}, \mathbf{V}, \mathbf{D})$ with respect to $\mathbf{X}$ and $\mathbf{V}$ followed by an update of $\mathbf{D}$ in three consecutive steps

$$\begin{cases} \mathbf{X}^{(t+1)} \leftarrow \arg\min_{\mathbf{X}} \mathcal{L}(\mathbf{X}, \mathbf{V}^{(t)}, \mathbf{D}^{(t)}) & \text{(16a)} \\ \mathbf{V}^{(t+1)} \leftarrow \arg\min_{\mathbf{V}} \mathcal{L}(\mathbf{X}^{(t+1)}, \mathbf{V}, \mathbf{D}^{(t)}) & \text{(16b)} \\ \mathbf{D}^{(t+1)} \leftarrow \mathbf{D}^{(t)} - \mathbf{G}\mathbf{X}^{(t+1)} - \mathbf{B}\mathbf{V}^{(t+1)} & \text{(16c)} \end{cases}$$

until some stopping criterion is satisfied. Specifically, $\mathbf{X}$, $\mathbf{V}$, and $\mathbf{D}$ can be computed as follows. The solution of $\mathbf{X}$ is derived from a reduced quadratic optimization problem of (16a), given

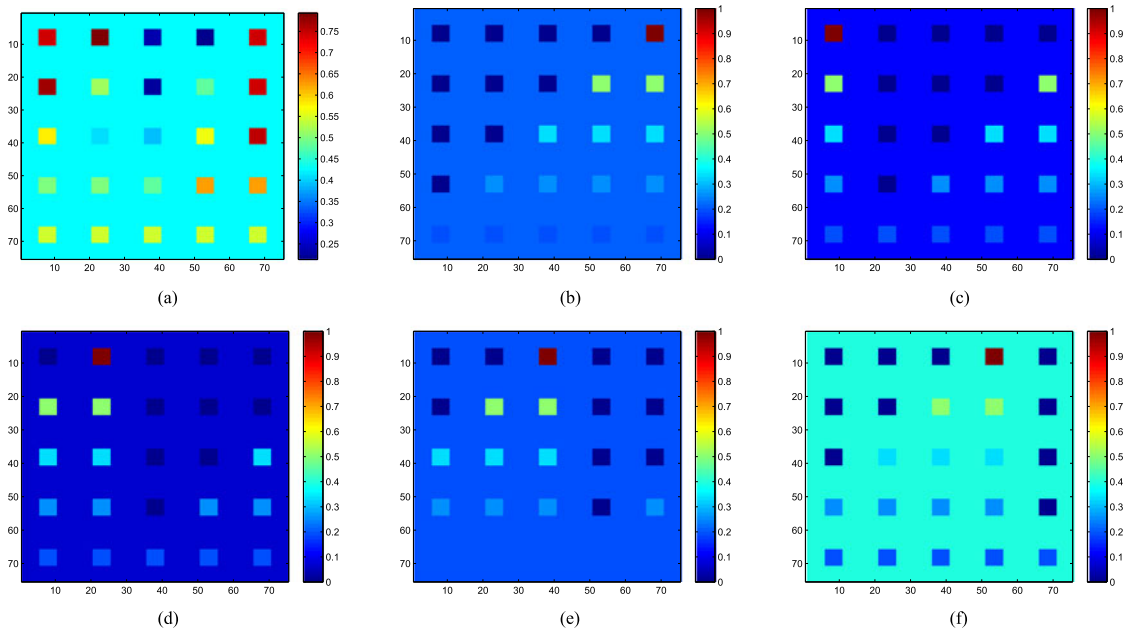

Fig. 3. DC1 and its related true fractional abundances for five endmembers: (a) synthetic image, (b) abundances of endmember 1, (c) abundances of endmember 2, (d) abundances of endmember 3, (e) abundances of endmember 4, and (f) abundances of endmember 5.

by

$$\mathbf{X}^{(t+1)} = (\mathbf{A}^T\mathbf{A} + 3\mathbf{I})^{-1}\left(\mathbf{A}^T\left(\mathbf{V}_1^{(t)} + \mathbf{D}_1^{(t)}\right) + \left(\mathbf{V}_2^{(t)} + \mathbf{D}_2^{(t)}\right) + \left(\mathbf{V}_3^{(t)} + \mathbf{D}_3^{(t)}\right) + \left(\mathbf{V}_4^{(t)} + \mathbf{D}_4^{(t)}\right)\right) \tag{17}$$

where $\mathbf{I}$ is the identity matrix, and the superscript character T denotes the transpose operator. Since $\mathbf{V}_1$, $\mathbf{V}_2$, $\mathbf{V}_3$, and $\mathbf{V}_4$ are fully separable in (16b), the minimization can be implemented in a component-wise manner. From (16b), it is easy to derive

$$\mathbf{V}_1^{(t+1)} = \frac{1}{1+\mu}\left[\mathbf{Y} + \mu\left(\mathbf{A}\mathbf{X}^{(t+1)} - \mathbf{D}_1^{(t)}\right)\right]. \tag{18}$$

As for $\mathbf{V}_2$, the closed-form solution [19] is explicitly given by

$$\mathbf{V}_2^{(t+1)} = T_{\text{row}}^{\text{VST}}\left(\mathbf{X}^{(t+1)} - \mathbf{D}_2^{(t)}, \frac{\lambda}{\mu}\right) \tag{19}$$

where $T_{\text{row}}^{\text{VST}}(\mathbf{U}, \tau)$ denotes the row-by-row implementation of the vectorial soft-threshold function $\mathbf{b} \to \mathbf{u}(\max\{\|\mathbf{u}\|_2 - \tau, 0\}/(\max\{\|\mathbf{u}\|_2 - \tau, 0\} + \tau))$ [31], [32] for a matrix $\mathbf{U}$. The optimization of $\mathbf{V}_3$ is solving an l_1-norm minimization, such that the shrinkage operator [33], [34] is utilized to obtain

$$\mathbf{V}_3^{(t+1)} = soft\left(\mathbf{X}^{(t+1)} - \mathbf{D}_3^{(t)} - \widehat{\mathbf{X}}^{(t)}, \frac{\gamma}{\mu}\right) + \widehat{\mathbf{X}}^{(t)} \tag{20}$$

in which $soft(\mathbf{U}, \tau)$ is a component-wise application of the soft-threshold function $u \to \text{sign}(u)\max\{|u| - \tau, 0\}$. The proof process of (20) is detailed in Appendix A. The value of $\mathbf{V}_4$ is given by [20], [19]

$$\mathbf{V}_4^{(t+1)} = \max\left(\mathbf{X}^{(t+1)} - \mathbf{D}_4^{(t)}, 0\right). \tag{21}$$

Algorithm 1: Proposed CCSU Algorithm.

Initialization
  set $t = 0$, choose K, h, μ, λ and γ
  initialize $\mathbf{X}^{(\mathbf{0})}$, $\mathbf{V}^{(0)}$ and $\mathbf{D}^{(0)}$
  search for $\Omega_j^{(0)}$ in $\mathbf{Y}$ for $\forall j$ according to (6)
  compute $\mathbf{W}^{(0)}$ with (9)
  compute $\widehat{\mathbf{X}}^{(0)}$ of $\mathbf{X}^*$ using (8)
repeat
  compute $\mathbf{X}^{(t+1)}$ according to (17)
  compute $\mathbf{V}^{(t+1)} = (\mathbf{V_1}^{(t+1)}, \mathbf{V_2}^{(t+1)}, \mathbf{V_3}^{(t+1)}, \mathbf{V_4}^{(t+1)})$ with (18)-(21) successively
  update $\mathbf{D}^{(t+1)} = (\mathbf{D_1}^{(t+1)}, \mathbf{D_2}^{(t+1)}, \mathbf{D_3}^{(t+1)}, \mathbf{D_4}^{(t+1)})$ using (22)
  update $\mathbf{Z}^{(t+1)}$ with $\mathbf{Z}^{(t+1)} = \mathbf{A}\mathbf{X}^{(t+1)}$
  search for $\Omega_j^{(t+1)}$ in $\mathbf{Z}^{(t+1)}$ for $\forall j$ according to (6)
  recompute $\mathbf{W}^{(t+1)}$ and $\widehat{\mathbf{X}}^{(t+1)}$ using (9) and (8)
  $t = t + 1$
until some stopping criterion is satisfied.

The following step is to update all the scaled Lagrange multipliers with

$$\begin{cases} \mathbf{D}_1^{(t+1)} &= \mathbf{D}_1^{(t)} - \mathbf{A}\mathbf{X}^{(t+1)} + \mathbf{V}_1^{(t+1)} \\ \mathbf{D}_i^{(t+1)} &= \mathbf{D}_i^{(t)} - \mathbf{X}^{(t+1)} + \mathbf{V}_i^{(t+1)}, i = 2, 3, 4. \end{cases} \tag{22}$$

The algorithmic procedure of the proposed method which uses CCSU to couple sparse unmixing and abundance estimation error reduction for hyperspectral data is formally stated in Algorithm 1. As for the stopping criterion, we make use of the

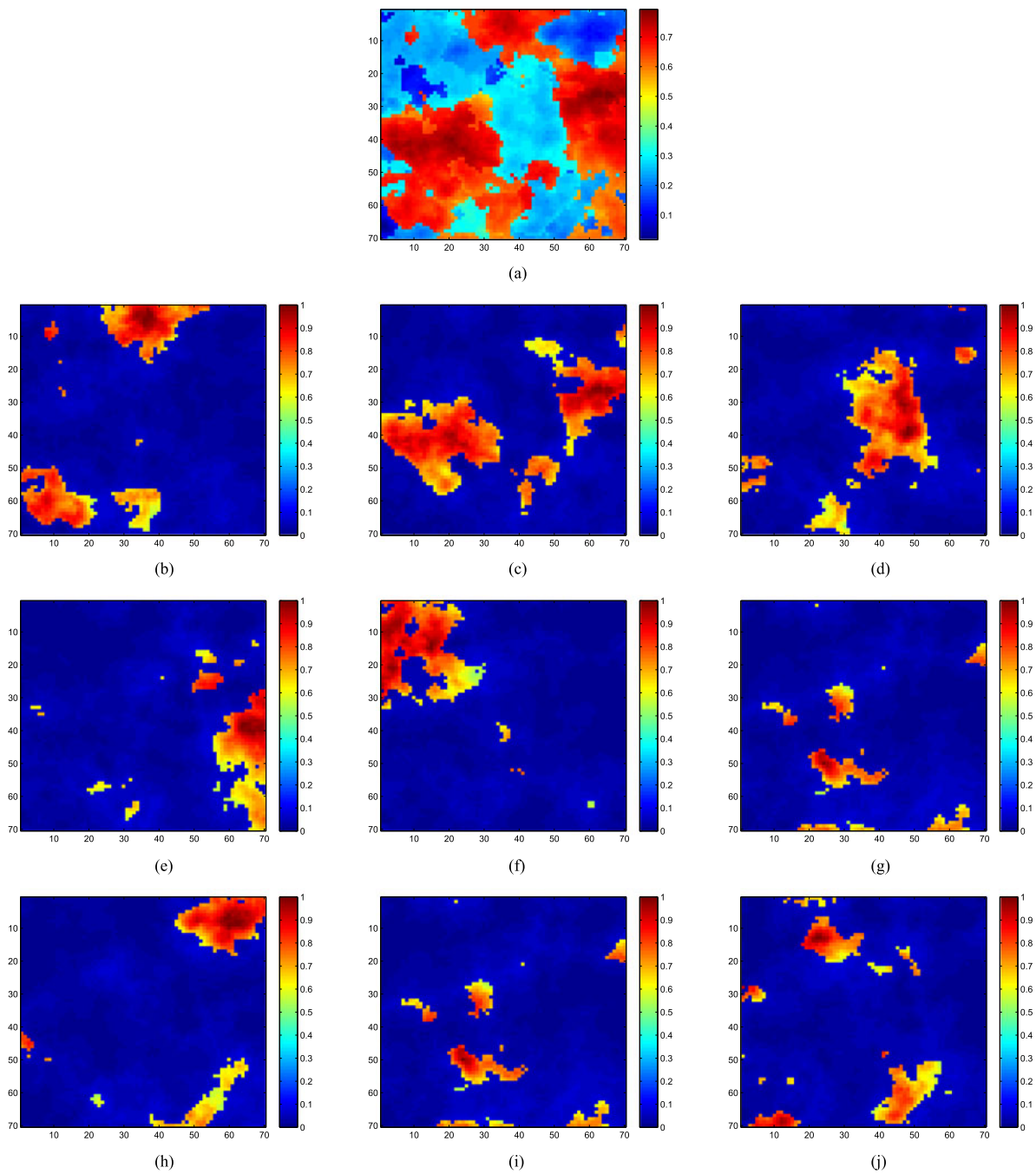

Fig. 4. DC2 and its related true fractional abundances for nine endmembers: (a) synthetic image, (b) abundances of endmember 1, (c) abundances of endmember 2, (d) abundances of endmember 3, (e) abundances of endmember 4, (f) abundances of endmember 5, (g) abundances of endmember 6, (h) abundances of endmember 7, (i) abundances of endmember 8, and (j) abundances of endmember 9.

maximum iteration number and $\|\mathbf{G}\mathbf{U}^{(t)} + \mathbf{B}\mathbf{V}^{(t)}\|_F < \varepsilon$, but only one of them is required to be satisfied.

IV. Experimental Results and Discussion

In this section, unmixing experiments are performed on the synthetic and real hyperspectral images to illustrate the effectiveness of our proposed CCSU algorithm. Results of other state-of-the-art unmixing methods such as NCLS [4], SUnSAL [17], CLSUnSAL [19], and SUnSAL-TV [20] are given for comparison purpose.

A. Synthetic Data Experiments

The spectral library used in these synthetic image experiments is $\mathbf{A} \in \mathbb{R}^{224\times240}$, which is generated by selecting 240 different materials from the USGS library, being available online[1]. It comprises spectral signatures with reflectance values given in 224 spectral bands and distributed uniformly over the interval $0.4 - 2.5\mu$m. We generate the following two different simulated hyperspectral data cubes by using this library.

[1] http://speclab.cr.usgs.gov/spectral.lib06

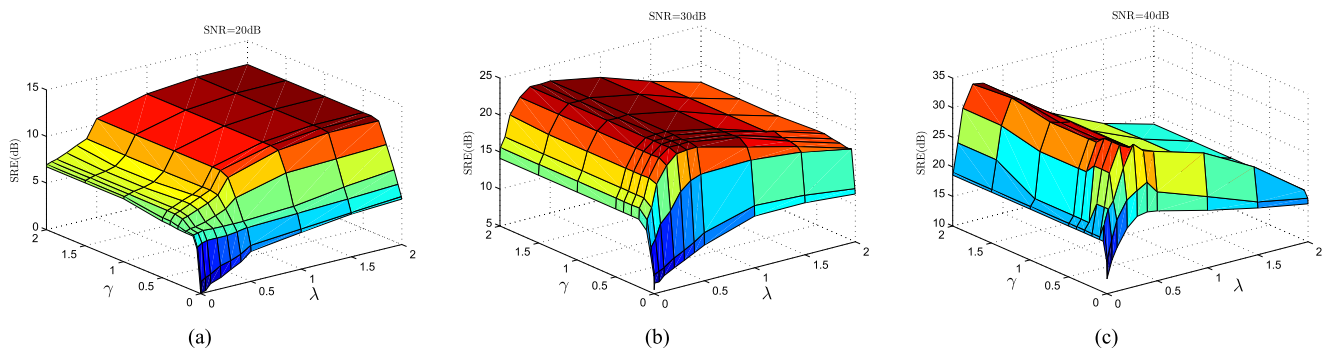

Fig. 5. SRE obtained by CCSU as a function of parameters λ and γ on the DC1 under different SNR levels: (a) SNR = 20 dB, (b) SNR = 30 dB, and (c) SNR = 40 dB.

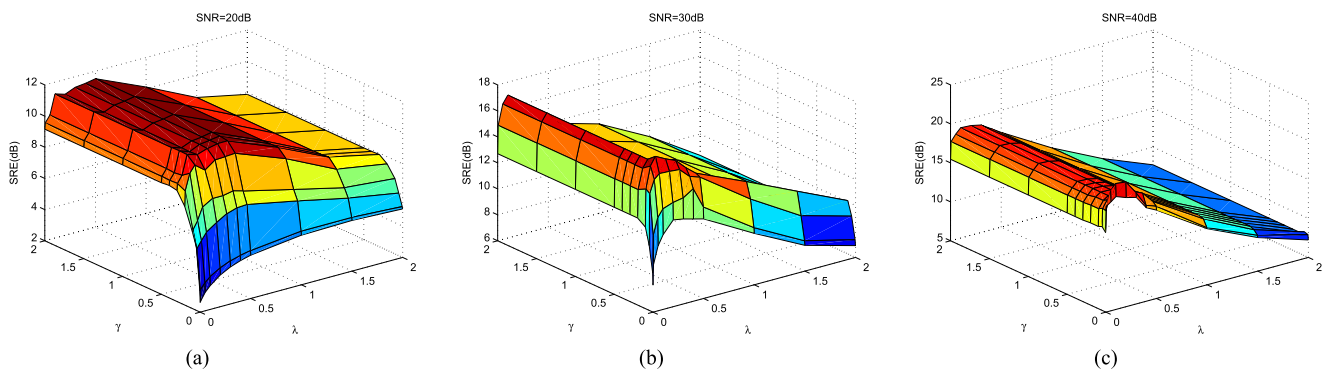

Fig. 6. SRE obtained by CCSU as a function of parameters λ and γ on the DC2 under different SNR levels: (a) SNR = 20 dB, (b) SNR = 30 dB, and (c) SNR = 40 dB.

TABLE I
PARAMETER SETTINGS FOR THE SYNTHETIC DATA

SNR	Algorithm	Parameter	DC1	DC2
20 dB	SUnSAL	λ	2e–1	1e–1
	CLSUnSAL	λ	2	1
	SUnSAL-TV	λ	5e–3	5e–3
		λ_{TV}	5e–2	5e–2
	CCSU	λ	1.5	0.5
		γ	0.4	0.4
30 dB	SUnSAL	λ	1e–1	5e–2
	CLSUnSAL	λ	2	0.5
	SUnSAL-TV	λ	5e–3	5e–4
		λ_{TV}	5e–3	5e–3
	CCSU	λ	0.5	0.1
		γ	0.3	0.1
40 dB	SUnSAL	λ	5e–3	5e–3
	CLSUnSAL	λ	0.5	0.05
	SUnSAL-TV	λ	5e–4	5e–4
		λ_{TV}	5e–3	5e–4
	CCSU	λ	0.2	0.05
		γ	0.05	0.1

1) *Simulated Data Cube 1* (DC1): We simulate the DC1 similar to as in [20], with 75×75 pixels and 224 bands. Five spectral signatures are randomly selected from the library $\mathbf{A}$ as the endmembers. In Fig. 3(a), there are pure regions as well as mixed regions constructed using mixtures ranging from two to five endmembers (from top to bottom), distributed spatially in the form of distinct square regions.

2) *Simulated Data Cube 2* (DC2): The abundance images of DC2 are created based on the Gaussian fields method [35], whose type is *Mattern*. Similarly, nine spectral signatures of $\mathbf{A}$ are randomly extracted as the endmembers to simulate the DC2 with the same number of bands as that of DC1, but composed of 70×70 pixels following the LMM. Fig. 4 shows the DC2 and its related true fractional abundances of nine endmembers. Obviously, the DC2 resembles the real scenario due to the spatial variability in abundances.

We add Gaussian noise into the above obtained data cubes with three different levels of the signal-to-noise ratio (SNR), i.e., 20, 30, and 40 dB.

Besides the visual interpretation, two objective metrics [18], i.e., the signal-to-reconstruction error (SRE) and the probability of success p_s, are adopted for quantitative evaluation. Specifically, the SRE in decibels, given by $\text{SRE} = 10\log_{10}(E[\|\mathbf{x}\|_2^2]/E[\|\mathbf{x}-\widetilde{\mathbf{x}}\|_2^2])$, measures the quality of the reconstruction of spectral mixtures, and p_s is defined as $p_s = P(\|\widetilde{\mathbf{x}}-\mathbf{x}\|^2/\|\mathbf{x}\|^2 \leq 3.16)$, giving an indication about the stability of the estimation, where $\widetilde{\mathbf{x}}$ is the estimation of the fractional abundance vector $\mathbf{x}$. Here, the choice of 3.16 means that the unmixing result is considered successful when $\|\widetilde{\mathbf{x}}-\mathbf{x}\|^2/\|\mathbf{x}\|^2 \leq 3.16$. This threshold was demonstrated in the previous work to provide satisfactory results [18]. The larger the both quantities are, the better the performance of the algorithm for recovering the abundances is. Six experiments

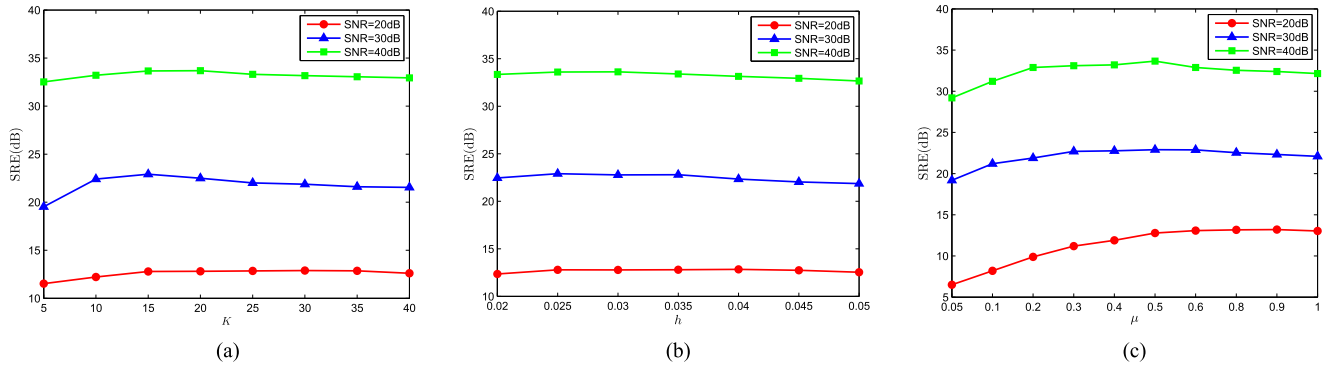

Fig. 7. SRE obtained by CCSU on the DC1 with respect to different parameters: (a) K, (b) h, and (c) μ.

TABLE II
SRE (IN DECIBELS) VALUES ON THE SYNTHETIC DATA

	Noise	NCLS	SUnSAL	CLSUnSAL	SUnSAL-TV	CCSU
DC1	$\mathbf{SNR} = 20$ dB	2.3675	3.4982	4.7750	10.8890	12.4267
	$\mathbf{SNR} = 30$ dB	7.3294	7.6253	12.2891	18.7212	22.9100
	$\mathbf{SNR} = 40$ dB	10.4596	15.7232	21.5225	28.1640	33.6695
DC2	$\mathbf{SNR} = 20$ dB	1.7683	5.3238	5.7104	8.0866	11.5120
	$\mathbf{SNR} = 30$ dB	7.4286	11.0013	11.9338	16.4257	17.6911
	$\mathbf{SNR} = 40$ dB	12.8895	16.7371	17.9520	19.9911	21.1396

TABLE III
p_s VALUES ON THE SYNTHETIC DATA

	Noise	NCLS	SUnSAL	CLSUnSAL	SUnSAL-TV	CCSU
DC1	$\mathbf{SNR} = 20$ dB	0.2944	0.3392	0.4724	0.9889	0.9962
	$\mathbf{SNR} = 30$ dB	0.5456	0.9596	0.9998	1	1
	$\mathbf{SNR} = 40$ dB	1	1	1	1	1
DC2	$\mathbf{SNR} = 20$ dB	0.1961	0.4152	0.7043	0.9889	0.9622
	$\mathbf{SNR} = 30$ dB	0.8071	0.9335	0.9493	0.9965	1
	$\mathbf{SNR} = 40$ dB	0.9784	1	1	1	1

are conducted on synthetic data to evaluate the proposed algorithm. Specifically, we first focus on the parameter settings, and then investigate the influence of noise, purity, the number of endmembers, as well as different spectral libraries, on unmixing performances. The last experiment aims at analyzing the convergence and computational complexity.

1) Experiment 1 (Parameter Settings): For the proposed CCSU algorithm, the involving parameters need to be determined before proceeding to the experiments. In specific implementation, the maximum number of iterations is set to 200. To reduce the computational complexity, the search of similar pixels and the update of $\widehat{\mathbf{X}}$ are performed in every 20 iterations, where we use the patch of size $3 \times 3 \times L$ to find out the similar pixels within an $11 \times 11 \times L$ search window. Also, we set $K = 15$, $h = 0.025$, $\mu = 0.5$, and tune λ and γ to achieve better unmixing performance. The algorithm is tested on both DC1 and DC2 using different values of the parameters λ and γ in a finite set $\{0.0005, 0.005, 0.05, 0.1, 0.2, 0.3, 0.4, 0.5, 1, 1.5, 2\}$.

Figs. 5 and 6 illustrate the SRE (in dB) of the proposed technique when these two parameters λ and γ vary under each SNR level. As can be seen, the use of a centralized constraint has the potential to efficiently improve the spectral unmixing performance, especially in the low SNR case. With the increase of the SNR, one should choose the relatively small values of λ and γ since there exits good fitness between $\mathbf{Y}$ and $\mathbf{AX}$. For the CCSU's performance, the $l_{2,1}$ mixed norm sparsity constraint is more dominant than the centralized constraint, and as λ is given, it shows some stability with respect to γ beyond a certain value. As such, from intuitive analysis and experimental results, λ and γ are set for both DC1 and DC2 at all considered SNR levels to give good results, see Table I. To make a fair comparison among the comparative methods, we have carefully tuned their parameters in the same finite set as given above to achieve the quasi-optimal performance.

Furthermore, we examine the effect of parameters K, h, and μ on the unmixing performance of the proposed CCSU algorithm. When analyzing one specific parameter, the other parameters are fixed as their corresponding chosen values. Fig. 7 shows the sensitivity of CCSU on DC1 with respect to different parameters, respectively. Three SRE curves shown in Fig. 7(a) first improve as K increases, and then begin to decrease slightly after the maximum value. By considering the tradeoff between performance and computational complexity, $K = 15$ is well accepted for all the cases of SNR. The similar variations can be observed in Fig. 7(c), and the choice of μ in high SNR case has less impact than in low SNR case. Comparatively speaking, CCSU shows the stable tendency in the unmixing performance with the change of h on the whole, as shown in Fig. 7(b).

2) Experiment 2 (Antinoise Capability): Tables II and III, respectively, report the SRE and p_s values obtained by applying different unmixing methods to all the synthetic hyperspectral data degraded by three different levels of noise. From both tables, we can observe that the overall performance of each unmixing method tends to degrade as the noise level increases. NCLS yields the worst unmixing performance, by only considering the nonnegative physical constraint. Moreover, as stated in [19] and [20], CLSUnSAL and SUnSAL-TV outperform SUnSAL due to the benefits of incorporating the subspace nature and spatial-contextual information of the hyperspectral data, respectively. In addition, the proposed CCSU algorithm performs

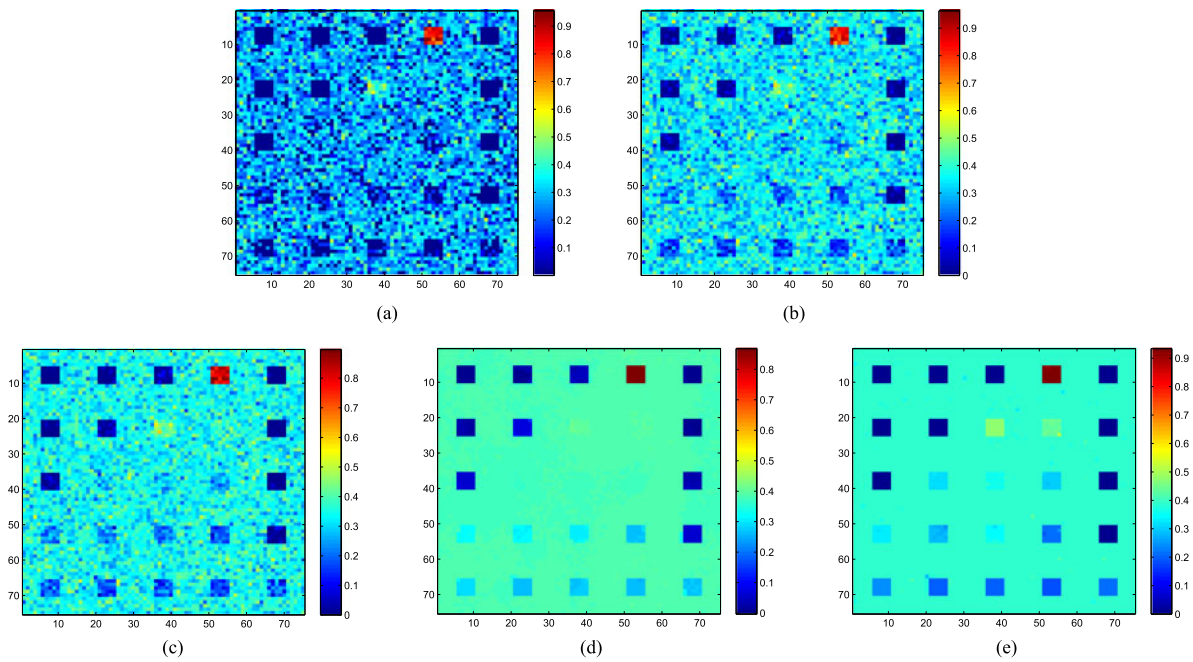

Fig. 8. Abundance maps obtained by different unmixing methods for endmember 5 in DC1: (a) NCLS, (b) SUnSAL, (c) CSUnSAL, (d) SUnSAL-TV, and (e) CCSU.

better than the others in all the cases for the quantitative metrics (i.e., SRE and p_s). This is because the proposed unmixing method considers abundance estimation error reduction during the procedure of unmixing.

For visual comparison, we take the case of SNR=20 dB as an example, and show the abundance maps estimated by five unmixing methods for the endmember 5 of DC1 in Fig. 8. Obviously, Fig. 8(a) and (b) looks noisy. Although the line sparsity constraint promotes the solutions of CLSUnSAL, Fig. 8(c) is still noisy. SUnSAL-TV imposes spatial consistency to significantly improve the quality of unmixing results, but it will oversmooth the abundances due to the piecewise constant assumption. CCSU provides much better estimation which are more similar to the ground-truth values [see Figs. 8(e) and 3(f)]. Moreover, from Fig. 9, it can be seen that CCSU and SUnSAL-TV have better antinoise capabilities than NCLS, SUnSAL, and CLSUnSAL, which indicates that the use of spatial information can alleviate the influence of noise on the sparse unmixing algorithms. The results shown in Fig. 9(m)–(o) reveal that CCSU achieves the best quality of abundance recovery, whereas SUnSAL-TV will yield some distortion in transition regions and structural details [see Fig. 9(j)–(l)].

3) Experiment 3 (Robustness Analysis to Purity): This experiment aims to comparatively analyze the robustness of four sparse unmixing algorithms to purity, since the mixing degrees in real hypespectral images vary from image to image. To this end, we take the DC2 as an example, and change the purity level from 1 to 0.6 for all considered SNR levels while keeping the number of endmembers together with the image size being fixed as that in the previous experiments. Fig. 10 shows the performance of each method on DC2 with different purities. We can observe that all algorithms present increasingly better unmixing results when the purity level approaches to 1. Meanwhile, CCSU outperforms other three sparse unmixing algorithms, showing its robustness to the highly mixed hyperspectral data.

4) Experiment 4 (Generalization to the Number of Endmembers): This experiment is taken to evaluate the unmixing performance of different algorithms when the synthetic data are generated by different numbers of endmembers. The DC2 is degraded by three levels of Gaussian noise (i.e., SNR=20, 30, and 40 dB) and generated by various numbers of endmembers with varying from 3 to 9, whose corresponding results are shown in Fig. 11. The higher the endmember number is, the more the difficulty for the hyperspectral image unmixing is. As shown in Fig. 11, the SREs of these four algorithms decline gradually when the number of endmembers increases, which is consistent with the observation discussed in [19]. This indicates that the sparsity of the solution can mitigate the sparse unmixing limitations caused by the usually high correlation of the spectral library. Nevertheless, CCSU can always obtain better estimation of the abundances than SUnSAL-TV. Both CSUnSAL and SUnSAL perform relatively worse, giving the smaller SRE values.

5) Experiment 5 (Impact of Different Spectral Libraries): In this experiment, we test the impact of different spectral libraries on various sparse unmixing algorithms. Here, three libraries (i.e., $\mathbf{A}_0$, $\mathbf{A}_1$, and $\mathbf{A}_2$) are utilized, where $\mathbf{A}_0 \in \mathbb{R}^{224 \times 498}$ refer to the original USGS library, $\mathbf{A}_1 \in \mathbb{R}^{224 \times 240}$ is exactly the library $\mathbf{A}$ used in the previous experiments, and $\mathbf{A}_2 \in \mathbb{R}^{224 \times 117}$ denotes the refined version of $\mathbf{A}_0$ by restricting spectral angles between the signatures of $\mathbf{A}_2$ equal to 7. Fig. 12 shows the SRE values obtained by each method with three spectral libraries on DC2 under different levels of SNR. According to Fig. 12, we can summarize that CCSU performs better on each library no matter how the SNR varies, further verifying the importance of simultaneously taking abundance estimation error reduction and nonlocal spatial information into account. In addition, the

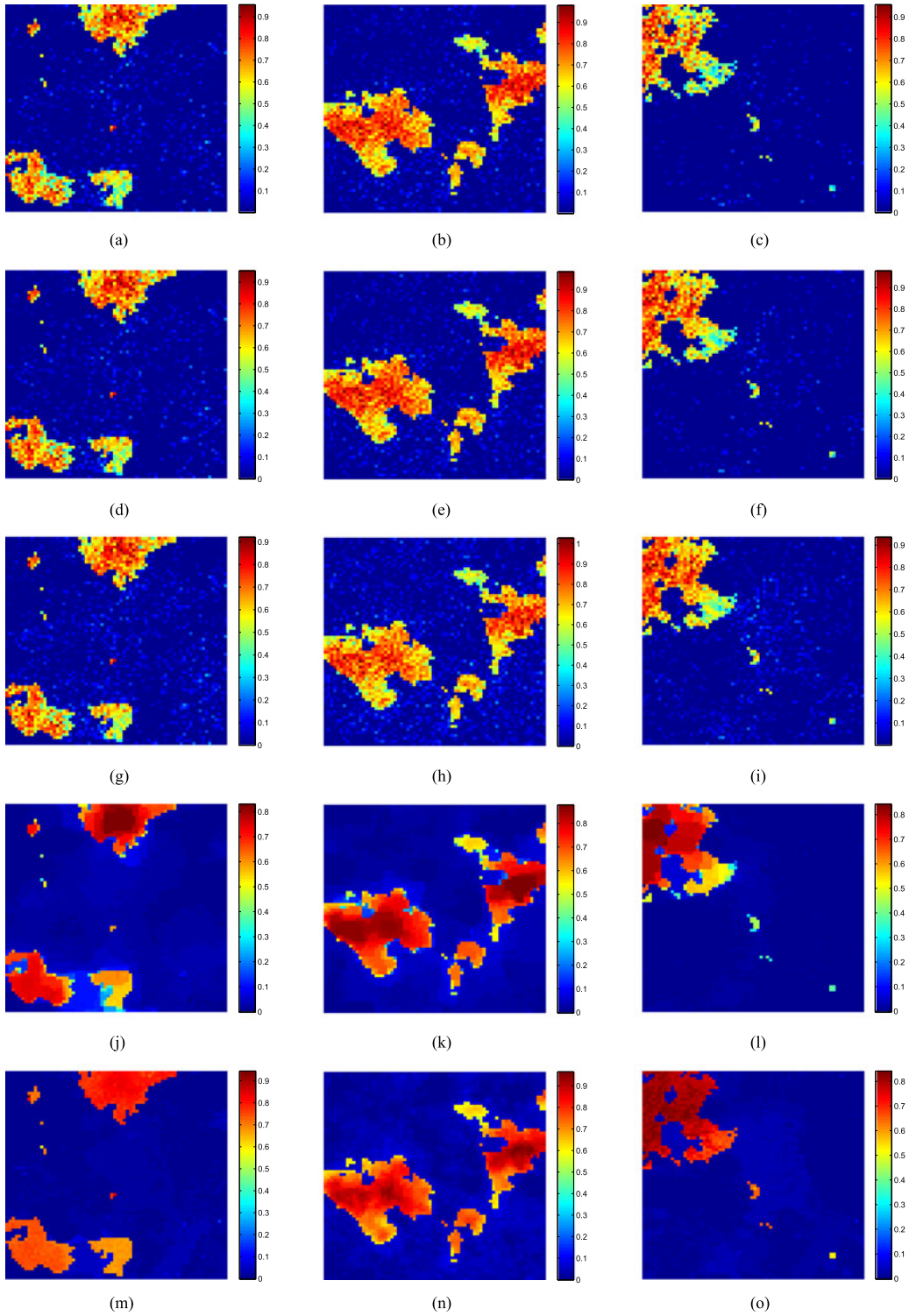

Fig. 9. Abundance maps obtained by different unmixing methods in DC2. From left to right: corresponding to the first, second, and fifth endmembers, respectively. From top to bottom: NCLS, SUnSAL, CSUnSAL, SUnSAL-TV, and CCSU.

proposed unmixing methods perform increasingly better when using $\mathbf{A}_0$, $\mathbf{A}_1$, and $\mathbf{A}_2$, respectively. The reason is that the mutual coherence of three libraries progressively becomes weaker, since $\mathbf{A}_1$ and $\mathbf{A}_2$ are two subsets of $\mathbf{A}_0$ (having its mutual coherence close to 1), especially where the spectral signatures of $\mathbf{A}_2$ can be regarded as quite different ones.

6) Experiment 6 (Convergence Analysis and Computational Complexity): The goal of this experiment is to analyze the convergence and computational complexity. As is known, all the four sparse unmixing algorithms adopt the ADMM to solve the underlying optimization problems. Therefore, as far as the convergence is concerned, it can be guaranteed from [29, Th. 8]

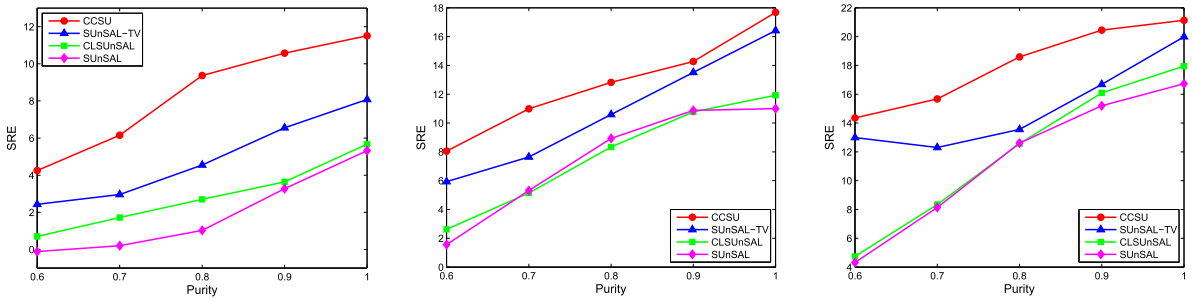

(a) (b) (c)

Fig. 10. Comparison of SUnSAL, CLSUnSAL, SUnSAL-TV and CCSU on DC2 in terms of SRE with respect to the purity level for all considered SNR levels: (a) SNR = 20 dB, (b) SNR = 30 dB, and (c) SNR = 40 dB.

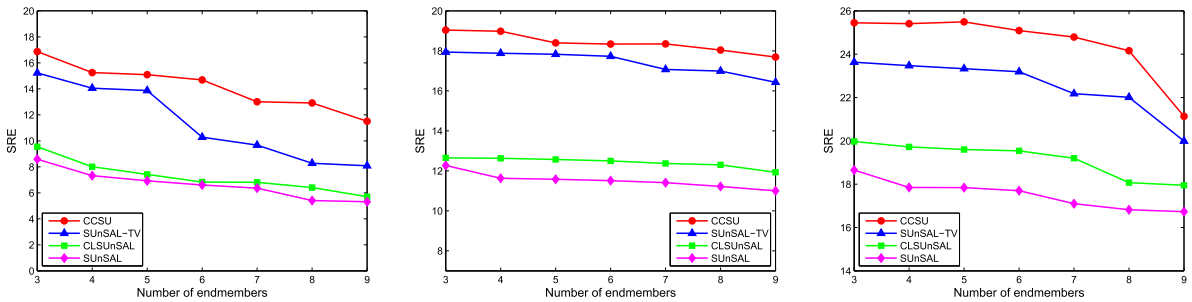

(a) (b) (c)

Fig. 11. Comparison of SUnSAL, CLSUnSAL, SUnSAL-TV, and CCSU on DC2 in terms of SRE with respect to the number of endmembers for all considered SNR levels: (a) SNR = 20 dB, (b) SNR = 30 dB, and (c) SNR = 40 dB.

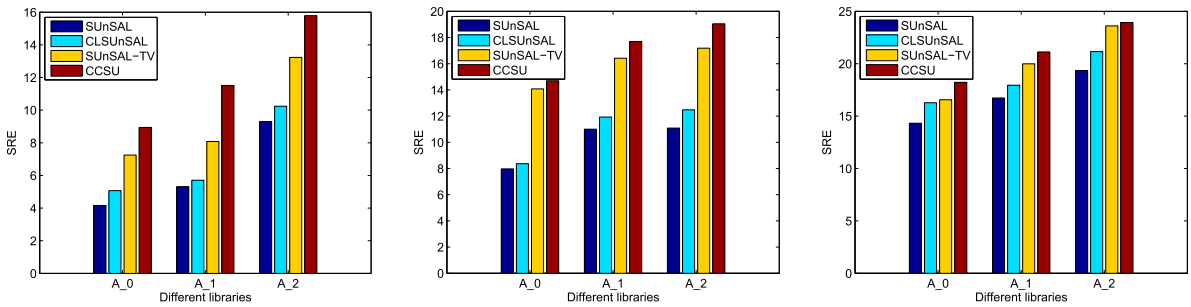

(a) (b) (c)

Fig. 12. Comparison of SUnSAL, CLSUnSAL, SUnSAL-TV, and CCSU on DC2 in terms of SRE with respect to different spectral libraries for all considered SNR levels: (a) SNR = 20 dB, (b) SNR = 30 dB, and (c) SNR = 40 dB.

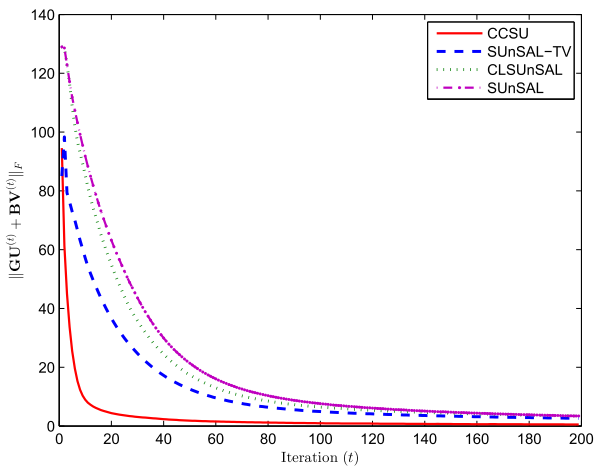

Fig. 13. Convergence curves of four sparse unmixing algorithms on DC2 at SNR = 20 dB.

TABLE IV
PARAMETER SETTINGS FOR REAL DATA

Algorithm	Parameter	Value
CLSUnSAL	λ	0.5
SUnSAL-TV	λ	1e− 3
	λ_{TV}	1e− 3
CCSU	λ	0.2
	γ	0.1

since each $\mathbf{G}$ matrix has full column rank, and all involved functions in $g(\mathbf{V})$ are closed, proper, and convex. To visually illustrate the convergence, Fig. 13 plots the $\|\mathbf{GU}^{(t)}+\mathbf{BV}^{(t)}\|_F$ curves of these four algorithms on DC2 at SNR=20 dB. By comparing their convergence curves, we can see that CCSU provides the smallest $\|\mathbf{GU}^{(t)}+\mathbf{BV}^{(t)}\|_F$ value, and it has

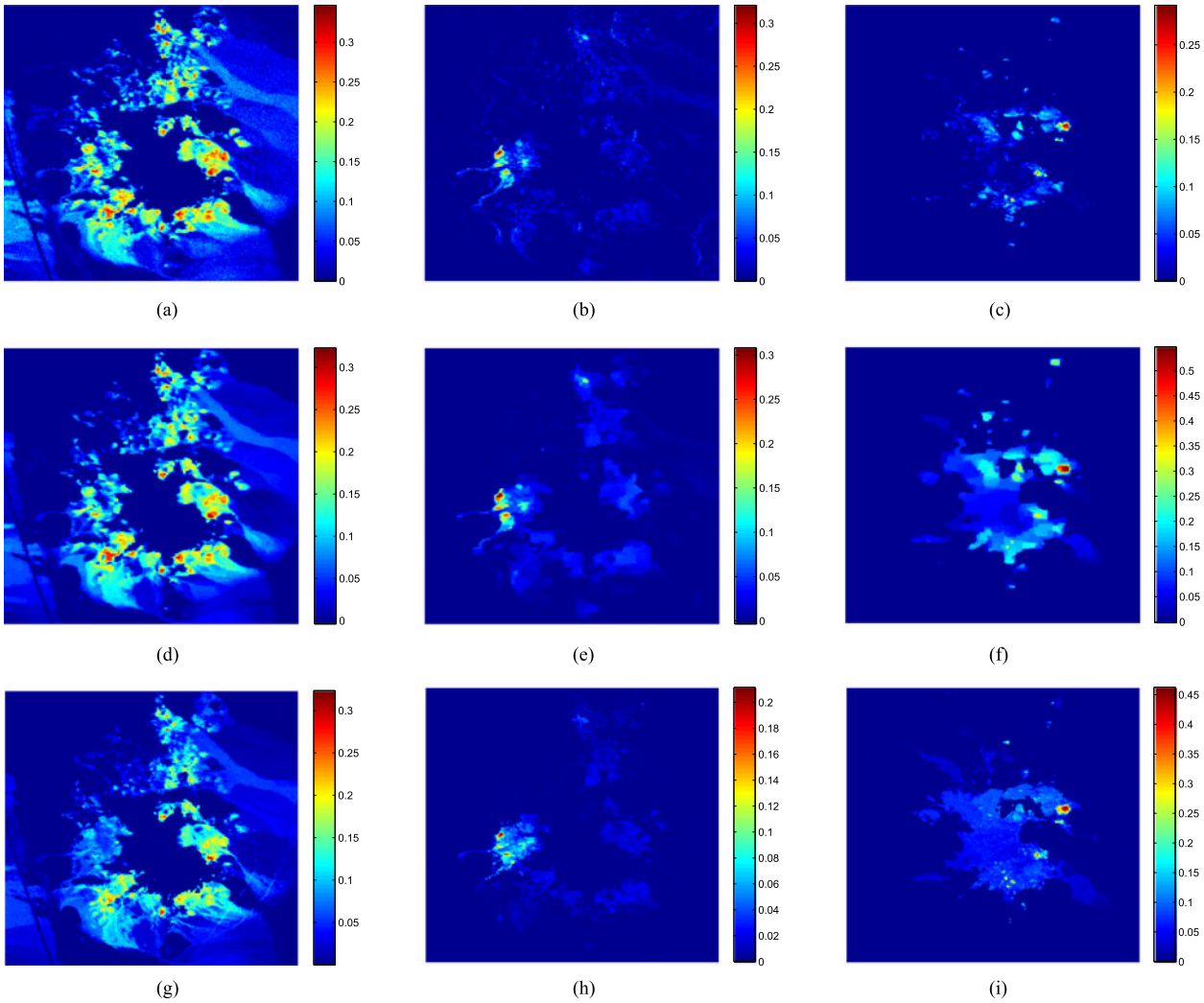

Fig. 14. Fractional abundance maps estimated for the AVIRIS Cuprite subscene. From left to right: Alunite, Buddingtonite, and Chalcedony. From top to bottom: CLSUnSAL, SUnSAL-TV, and CCSU.

faster convergence speed than SUnSAL, CLSUnSAL, and SUnSAL-TV.

Next, the computational complexity of four sparse unmixing algorithms is comparatively analyzed. To this end, we make use of the CPU execution time of programs to estimate it. All the algorithms are implemented in MATLAB R2010b on a desktop computer with Intel Pentium CPU G2020 (2.90 GHz) and 2-GB RAM. For the SUnSAL, CLSUnSAL, and SUnSAL-TV algorithms, the average computational times of three levels of noise are about 64, 65, and 199 s, respectively. As far as CCSU is concerned, the main computational demand lies in the search of nonlocal similar patches, for which a MEX file including one built-in subroutine in C programming is called to improve the efficiency of its MATLAB program. The corresponding average time is 631 s for three levels of noise. It is obvious that CCSU has highest computational cost due to the exploitation of nonlocal redundancy of abundance map, followed by SUnSAL-TV. Only analyzing the hyperspectral data without incorporating spatial information, SUnSAL and CLSUnSAL require less running time. Besides the inferiority of computational complexity, more importantly CCSU achieves the better unmixing performance. In practice, the general-purpose graphics processing units (GPUs) can be adopted to greatly accelerate the CCSU algorithm.

B. Real Data Experiments

The real hyperspectral image is a subscene of the well-known AVIRIS Cuprite data set, having 250×190 pixels and 188 bands with the removal of water absorption and low SNR bands. The spectral library used here is $\mathbf{A} \in \mathbb{R}^{188 \times 498}$ from the USGS library with the corresponding bands removed. Prior to unmixing, the band-dependent correction strategy [18] is utilized to minimize the mismatches between the real pixel spectra and that available in the library. The same parameters are used as that mentioned in Section IV-A except $h = 0.01$, $\mu = 0.05$, and all regularization parameters of CLSUnSAL, SUnSAL-TV, and CCSU are listed in Table IV. Because the true abundances of the real hyperspectral data are unavailable, we just can make a qualitative analysis with reference to the distribution map of minerals provided online.[2] Fig. 14 shows the abundance maps

[2]http://speclab.cr.usgs.gov/cuprite95.tgif.2.2um_map.gif

of three dominant materials (i.e., Alunite, Buddingtonite, and Chalcedony) in the scene estimated by CLSUnSAL, SUnSAL-TV, and CCSU. As evidenced from Fig. 14, three algorithms have shown the acceptable unmixing results, with high abundances at the pixels showing the existence of the minerals. However, CLSUnSAL yields the abundance maps without good spatial consistency of minerals of interest, and has some more inaccurate abundance estimates which are obvious in the abundance maps corresponding to Buddingtonite and Chalcedony [i.e., Fig. 14(b) and (c)]. Meanwhile, the estimated abundances by SUnSAL-TV may exhibit an oversmooth visual effect. Compared with CLSUnSAL and SUnSAL-TV, our proposed CCSU is more effective for sparse unmixing.

V. Conclusion

In this paper, we proposed a CCSU algorithm for hyperspectral images. A main contribution of this proposed algorithm is to suppress abundance estimation error which is defined in our paper. It is unavoidable in traditional sparse unmixing methods and will affect the accuracy of unmixing results. To minimize the abundance estimation error, from a different perspective, we introduced a centralized sparsity constraint and coupled it with sparse unmixing together. Experimental results have demonstrated that the proposed CCSU algorithm can unmix the hyperspectral data more effectively against NCLS, SUnSAL, CLSUnSAL, and SUnSAL-TV. Future work will be devoted to automatically determining the underlying regularization parameters under a Bayesian inference framework.

Appendix A
Mathematical Proof of (20)

To compute $\mathbf{V_3}$, the optimization problem to be solved is

$$\mathbf{V_3}^{(t+1)} \leftarrow \arg\min_{\mathbf{V_3}} \gamma\|\mathbf{V_3} - \widehat{\mathbf{X}}^{(t)}\|_1 + \frac{\mu}{2}\|\mathbf{X}^{(t+1)} - \mathbf{V}_3 - \mathbf{D}_3^{(t)}\|_F^2. \quad (23)$$

The formula (23) can be rewritten as follows:

$$\mathbf{V_3}^{(t+1)} \leftarrow \arg\min_{\mathbf{V_3}} \gamma\|\mathbf{V_3} - \widehat{\mathbf{X}}^{(t)}\|_1 + \frac{\mu}{2}\|\mathbf{X}^{(t+1)} - (\mathbf{V}_3 - \widehat{\mathbf{X}}^{(t)}) - \widehat{\mathbf{X}}^{(t)} - \mathbf{D}_3^{(t)}\|_F^2 \quad (24)$$

whose solution is the well-known soft threshold [31], i.e.,

$$\mathbf{V_3}^{(t+1)} - \widehat{\mathbf{X}}^{(t)} = soft\Big(\mathbf{X}^{(t+1)} - \widehat{\mathbf{X}}^{(t)} - \mathbf{D}_3^{(t)}, \frac{\gamma}{\mu}\Big). \quad (25)$$

At last, we have

$$\mathbf{V}_3^{(t+1)} = soft\Big(\mathbf{X}^{(t+1)} - \mathbf{D}_3^{(t)} - \widehat{\mathbf{X}}^{(t)}, \frac{\gamma}{\mu}\Big) + \widehat{\mathbf{X}}^{(t)}. \quad (26)$$

This completes the mathematical proof of (20).

Acknowledgment

The authors would like to thank the IEEE Staff Editor, AndreAnna McLean, for the detailed and careful edits.

References

[1] N. Keshava and J. F. Mustard, "Spectral unmixing," *IEEE Signal Process. Mag.*, vol. 19, no. 1, pp. 44–57, Jan. 2002.
[2] J. M. Bioucas-Dias, A. Plaza, N. Dobigeon, M. Perente, Q. Du, P. Gader, and J. Chanussot, "Hyperspectral unmixing overview: Geometrical statistical, and sparse-regression-based approaches," *IEEE J. Sel. Topics Appl. Earth Observ. Remote Sens.*, vol. 5, no. 2, pp. 354–379, Apr. 2012.
[3] N. Dobigeon, J. Y. Tourneret, C. Richard, J. C. M. Bermudez, S. McLaughlin, and A. O. Hero, "Nonlinear unmixing of hyperspectral images: models and algorithms," *IEEE Signal Process. Mag.*, vol. 31, no. 1, pp. 82–94, Jan. 2014.
[4] D. C. Heinz and C. I. Chang, "Fully constrained least squares linear spectral mixture analysis method for material quantification in hyperspectral imagery," *IEEE Trans. Geosci. Remote Sens.*, vol. 39, no. 3, pp. 529–545, Mar. 2001.
[5] M. E. Winter, "N-FINDR: An algorithm for fast autonomous spectral endmember determination in hyperspectral data," in *Proc. SPIE Conf. Imaging Spectrom. V*, Pasadena, USA, 1999, pp. 266–275.
[6] J. M. P. Nascimento and J. M. Bioucas-Dias, "Vertex component analysis: A fast algorithm to unmix hyperspectral data," *IEEE Trans. Geosci. Remote Sens.*, vol. 43, no. 4, pp. 898–910, Apr. 2005.
[7] J. Li and J. M. Bioucas-Dias, "Minimum volume simplex analysis: A fast algorithm to unmix hyperspectral data," in *Proc. Int. Geosci. Remote Sens. Symp.*, Boston, MA, USA, 2008, pp. 250–253.
[8] T. H. Chan, C. Y. Chi, Y. M. Huang, and W. K. Ma, "A convex analysis-based minimum-volume enclosing simplex algorithm for hyperspectral unmixing," *IEEE Trans. Signal Process.*, vol. 57, no. 11, pp. 4418–4432, Nov. 2009.
[9] M. Craig, "Minimum-volume transforms for remotely sensed data," *IEEE Trans. Geosci. Remote Sens.*, vol. 32, no. 3, pp. 542–552, May 1994.
[10] N. Dobigeon, S. Moussaoui, M. Coulon, J. Y. Tourneret, and A. O. Hero, "Joint Bayesian endmember extraction and linear unmixing for hyperspectral imagery," *IEEE Trans. Signal Process.*, vol. 57, no. 11, pp. 4355–4368, Nov. 2009.
[11] J. Bayliss, J. A. Gualtieri, and R. F. Cromp, "Analyzing hyperspectral data with independent component anaysis," in *Proc. SPIE 26th AIPR Workshop*, Washington, DC, USA, 1997, pp. 133–143.
[12] V. P. Pauca, J. Piper, and R. J. Plemmons, "Nonnegative matrix factorization for spectral data analysis," *Linear Algebra Appl.*, vol. 416, no. 1, pp. 29–47, Jan. 2006.
[13] L. D. Miao and H. R. Qi, "Endmember extraction from highly mixed data using minimum volume constrained nonnegative matrix factorization," *IEEE Trans. Geosci. Remote Sens.*, vol. 45, no. 3, pp. 765–777, Mar. 2007.
[14] Y. T. Qian, S. Jia, J. Zhou, and A. Robles-Kelly, "Hyperspectral unmixing via $L_{1/2}$ sparsity-constrained nonnegative matrix factorization," *IEEE Trans. Geosci. Remote Sens.*, vol. 49, no. 11, pp. 4282–4297, Nov. 2011.
[15] N. Wang, B. Du, and L. P. Zhang, "An endmemeber dissimilarity constrained non-negative matrix factorization method for hyperspectral unmixing," *IEEE J. Sel. Top. Appl. Earth Observ. Remote Sens.*, vol. 6, no. 2, pp. 554–569, Apr. 2013.
[16] Y. Yuan, Y. C. Feng, and X. Q. Lu, "Projection-based NMF for hyperspectral unmixing," *IEEE J. Sel. Topics Appl. Earth Observ. Remote Sens.*, vol. 8, no. 6, pp. 2632–2643, Jun. 2015.
[17] J. M. Bioucas-Dias and M. A. T. Figueiredo, "Alternating direction algorithms for constrained sparse regression: Application to hyperspectral unmixing," in *Proc. 2nd Workshop Hyperspectral Image Signal Process., Evol. Remote Sens.*, Reykjavik, Iceland, 2010, pp. 1–4.
[18] M. D. Iordache, J. M. Bioucas-Dias, and A. Plaza, "Sparse unmixing of hyperspectral data," *IEEE Trans. Geosci. Remote Sens.*, vol. 49, no. 6, pp. 2014–2039, Jun. 2011.
[19] M. D. Iordache, J. M. Bioucas-Dias, and A. Plaza, "Collaborative sparse regression for hyperspectral unmixing," *IEEE Trans. Geosci. Remote Sens.*, vol. 52, no. 1, pp. 341–354, Jan. 2014.
[20] M. D. Iordache, J. M. Bioucas-Dias, and A. Plaza, "Total variation spatial regularization for sparse hyperspectral unmixing," *IEEE Trans. Geosci. Remote Sens.*, vol. 50, no. 11, pp. 4484–4502, Nov. 2012.
[21] Y. F. Zhong, R. Y. Feng, and L. P. Zhang, "Non-local sparse unmixing for hyperspectral remote sensing imagery," *IEEE J. Sel. Topics Appl. Earth Observ. Remote Sens.*, vol. 7, no. 6, pp. 1889–1909, Jun. 2014.
[22] R. Y. Feng, Y. F. Zhong, and L. P. Zhang, "An improved nonlocal sparse unmixing algorithm for hyperspectral imagery," *IEEE Geosci. Remote Sens. Lett.*, vol. 12, no. 4, pp. 915–919, Apr. 2015.
[23] C. I. Chang and Q. Du, "Interference and noise-adjusted principal components analysis," *IEEE Trans. Geosci. Remote Sens.*, vol. 37, no. 5, pp. 2387–2396, Sep. 1999.

[24] A. Buades, B. Coll, and J. M. Morel, "A review of image denoising algorithms, with a new one," *Multiscale Model. Simul.*, vol. 4, no. 2, pp. 490–530, Mar. 2005.
[25] H. Y. Zhang, J. Y. Li, Y. C. Huang, and L. P. Zhang, "A nonlocal weighted joint sparse representation classification method for hyperspectral imagery," *IEEE J. Sel. Topics Appl. Earth Observ. Remote Sens.*, vol. 7, no. 6, pp. 2056–2065, Jun. 2014.
[26] Y. Q. Zhao, J. X. Yang, and J. C. W. Chan, "Hyperspectral imagery super-resolution by spatial–spectral joint nonlocal similarity," *IEEE J. Sel. Topics Appl. Earth Observ. Remote Sens.*, vol. 7, no. 6, pp. 2671–2679, Jun. 2014.
[27] W. S. Dong, L. Zhang, G. M. Shi, and X. Li, "Nonlocally centralized sparse representation for image restoration," *IEEE Trans. Image Process.*, vol. 22, no. 4, pp. 1620–1630, Apr. 2012.
[28] D. Gabay and B. Mercier, "A dual algorithm for the solution of nonlinear variational problems via finite element approximation," *Comput. Math. Appl.*, vol. 2, no. 1, pp. 17–40, Jan. 1976.
[29] J. Eckstein and D. P. Bertsekas, "On the Douglas–Rachford splitting method and the proximal point algorithm for maximal monotone operators," *Math. Program.*, vol. 55, no. 1–3, pp. 293–318, Apr. 1992.
[30] M. V. Afonso, J. M. Bioucas-Dias, and M. A. T. Figueiredo, "An augmented Lagrangian approach to the constrained optimization formulation of imaging inverse problems," *IEEE Trans. Image Process.*, vol. 20, no. 3, pp. 681–695, Mar. 2011.
[31] P. L. Combettes and V. R. Wajs, "Signal recovery by proximal forward–backward splitting," *SIAM J. Multiscale Model. Simul.*, vol. 4, no. 4, pp. 1168–1200, Nov. 2005.
[32] S. J. Wright, R. D. Nowak, and M. A. T. Figueiredo, "Sparse reconstruction by separable approximation," *IEEE Trans. Signal Process.*, vol. 57, no. 7, pp. 2479–2493, Jul. 2009.
[33] W. T. Yin, S. Osher, D. Goldfarb, and J. Darbon, "Bregman iterative algorithms for $l1$-minimization with applications to compressed sensing," *SIAM J. Imag. Sci.*, vol. 1, no. 1, pp. 143–168, Jan. 2008.
[34] J. F. Cai, S. Osher, and Z. W. Shen, "Convergence of the linearized Bregman iteration for $l1$-norm minimization," *Math. Comput.*, vol. 78, no. 268, pp. 2127–2136, Mar. 2009.
[35] B. Kozintsev, "Computations with Gaussian random fields," Ph.D. dissertation, Univ. Maryland, College Park, MD, USA, 1999.

Rui Wang received the B.Sc. and M.Sc. degrees in information engineering from Southwest Jiaotong University, Chengdu, China, in 2002 and 2008, respectively. She is currently working toward the Ph.D. degree in signal and information processing at the School of Information Science and Technology, Southwest Jiaotong University, Chengdu, China.

Her research interests include hyperspectral image analysis and processing.

Heng-Chao Li (S'06–M'08–SM'14) received the B.Sc. and M.Sc. degrees from the Southwest Jiaotong University, Chengdu, China, in 2001 and 2004, respectively, and the Ph.D. degree from the Graduate University of Chinese Academy of Sciences, Beijing, China, in 2008, all in information and communication engineering.

He is currently a Professor with the Sichuan Provincial Key Laboratory of Information Coding and Transmission, Southwest Jiaotong University, Chengdu, China. From November 2013 to October 2014, he was a Visiting Scholar working with Prof. W. J. Emery at the University of Colorado at Boulder, Boulder, CO, USA. His research interests include statistical analysis of synthetic aperture radar images, remote sensing image processing, and signal processing in communications.

Prof. Li received several scholarships or awards, especially including the Special Grade of the Financial Support from China Postdoctoral Science Foundation in 2009 and the New Century Excellent Talents in University from the Ministry of Education of China in 2011. In addition, he has also been a Reviewer for several international journals and conferences, such as the IEEE TRANSACTIONS ON GEOSCIENCE AND REMOTE SENSING, the IEEE JOURNAL OF SELECTED TOPICS IN APPLIED EARTH OBSERVATIONS AND REMOTE SENSING, the IEEE GEOSCIENCE AND REMOTE SENSING LETTERS, the IEEE TRANSACTIONS ON IMAGE PROCESSING, the *IET Radar, Sonar and Navigation*, and the *Canadian Journal of Remote Sensing*. He is currently serving as an Associate Editor of the IEEE JOURNAL OF SELECTED TOPICS IN APPLIED EARTH OBSERVATIONS AND REMOTE SENSING.

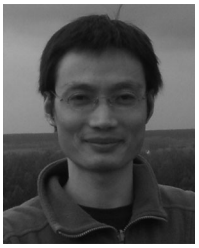

Wenzhi Liao (S'10–M'14–SM'16) received the B.Sc. degree in mathematics from Hainan Normal University, Haikou, China, in 2006, the Ph.D. degree in engineering from South China University of Technology, Guangzhou, China, in 2012, and the Ph.D. degree in computer science engineering from Ghent University, Ghent, Belgium, in 2012.

Since 2012, he has been a Postdoctoral Researcher at Ghent University. His current research interests include pattern recognition, remote sensing, and image processing. In particular, his interests include mathematical morphology, multitask feature learning, multisensor data fusion, and hyperspectral image restoration.

Dr. Liao is a member of the Geoscience and Remote Sensing Society (GRSS) and IEEE GRSS Data Fusion Technical Committee. He received the Best Paper Challenge Awards on both 2013 IEEE GRSS Data Fusion Contest and 2014 IEEE GRSS Data Fusion Contest.

Xin Huang (M'13–SM'14) received the Ph.D. degree in photogrammetry and remote sensing in 2009 from the State Key Laboratory of Information Engineering in Surveying, Mapping and Remote Sensing, Wuhan University, Wuhan, China.

He is currently a Full Professor with Wuhan University, where he teaches remote sensing, photogrammetry, image interpretation, etc. He is the Founder and Director of the Institute of Remote Sensing Information Processing, School of Remote Sensing and Information Engineering, Wuhan University. He has published more than 80 peer-reviewed articles in the international journals. His research interests include hyperspectral data analysis, high-resolution image processing, pattern recognition, and remote sensing applications.

Prof. Huang received the Top-Ten Academic Star of Wuhan University in 2009, the Boeing Award for the Best Paper in Image Analysis and Interpretation from the American Society for Photogrammetry and Remote Sensing in 2010, the New Century Excellent Talents in University from the Ministry of Education of China in 2011, the National Excellent Doctoral Dissertation Award of China in 2012, and the China National Science Fund for Excellent Young Scholars in 2015. In 2011, he was recognized by the IEEE Geoscience and Remote Sensing Society (GRSS) as the Best Reviewer of the IEEE GEOSCIENCE AND REMOTE SENSING LETTERS. He was the winner of the IEEE GRSS 2014 Data Fusion Contest. He was the Lead Guest Editor of the special issue on information extraction from high-spatial-resolution optical remotely sensed imagery for the IEEE JOURNAL OF SELECTED TOPICS IN APPLIED EARTH OBSERVATIONS AND REMOTE SENSING (vol. 8, no.5, May 2015), and the Lead Guest Editor of the special issue on sparsity-driven high dimensional remote sensing image processing and analysis for the *Journal of Applied Remote Sensing* (vol. 10, no. 4, Oct 2016). He has been an Associate Editor of the IEEE GEOSCIENCE AND REMOTE SENSING LETTERS since 2014 and of the *Photogrammetric Engineering and Remote Sensing* since 2016 .

Wilfried Philips (S'90–M'93–SM'10) was born in Aalst, Belgium, on October 19, 1966. He received the Diploma degree in electrical engineering and the Ph.D. degree in applied sciences both from Ghent University, Ghent, Belgium, in 1989 and 1993, respectively.

From October 1989 to October 1997, he was with the Department of Electronics and Information Systems, Ghent University, for the Flemish Fund for Scientific Research (FWO-Vlaanderen), first as a Research Assistant and later as a Postdoctoral Research Fellow. Since November 1997, he has been with the Department of Telecommunications and Information Processing, Ghent University, where he is currently a Full-Time Professor and is the Head of the research group "Image Processing and Interpretation," which is part of the Virtual Flemish Information and Communication Technology Research Institute iMinds. His research interests include image and video restoration, analysis and the modeling of image reproduction systems, remote sensing, surveillance, and industrial inspection.